Chapter 4

mRNA display selection of high affinity fibronectins that modulate SARS N protein *in vivo*

In collaboration with Hsiang-I Liao and Professor Ren Sun,
UCLA department of Molecular and Medical Pharmacology

Abstract

Severe Acute Respiratory Syndrome Coronavirus (SARS-CoV) nucleocapsid (N) protein has been shown to play important roles in both viral replication and in the modulation of host cell processes. Direct inhibition of N protein in live, virus infected cells may help elucidate the complex functions of N protein and further explore N as a therapeutic target. Using *in vitro* selection by mRNA display, we evolved novel protein affinity reagents based on the fibronectin type III domain that bind to SARS N protein and are functional *in vivo*. Six fibronectins recognize the C-terminal self-association domain, while two fibronectins require the N-terminal RNA binding domain for binding. One C-terminal specific affinity reagent binds with a K_d = 1.7 nM, and one N-terminal dependent fibronectin binds with a K_d = 72 nM. All eight binders characterized have highly dissimilar sequences and represent unique solution to the molecular recognition of N. Four fibronectins were highly functional *in vivo*; the best inhibit virus production over 1000-fold when transiently expressed prior to infection. Also, a synergistic effect in inhibition of viral gene production was measured in cells expressing two binders that recognize non-overlapping epitopes. In this study, we demonstrate the potential for mRNA display in the development of novel tools for cell biology. The diverse and stable high affinity fibronectins selected can be used for visualization and direct analysis of N protein function.

Introduction

The causative agent of the epidemic known as Severe Acute Respiratory Syndrome (SARS) was discovered to be a novel member of the *Coronaviridae* known as SARS-CoV (*1*). Prior to the discovery of SARS-CoV in 2003, only two human coronaviruses were known, together causing ~30% of common cold cases. Currently there are no effective antiviral agents against SARS-CoV, but many vaccine studies are ongoing. Coronaviruses are large enveloped, RNA viruses with an approximately 30-kb positive strand genome. The 5' two-thirds of the genome contain open reading frames 1a and 1b, which encode non-structural proteins that form the replication/transcription complex (RTC). The 3' one-third of the genome encodes the major structural proteins that are conserved in the coronavirus family: spike (S), envelope (E), membrane (M), and nucleocapsid (N) proteins, along with several group-specific accessory proteins.

N oligomerizes and packages the 29.7kb SARS-CoV genomic RNA to form the viral core. N protein, a 422 amino acid phosphoprotein, is composed of two structural domains linked by a non-structured domain. The N-terminal domain (NTD) is the putative genomic RNA binding domain (*2*), while the C-terminal domain (CTD) mediates self association (*3*). The CTD has also been shown to bind nucleic acid nonspecifically and may play an important role in genomic RNA packaging (*4*). The middle, unstructured domain interacts with the M protein, anchoring the membrane proteins to the viral core.

In addition to its important function in packaging genomic RNA, N protein plays important roles in both virus and host cell processes (*5*). N is predominantly localized in the cytoplasm but is also found in the nucleolus (*6*) and may be actively shuttled to and from the nucleus (*7*). N binds nucleic acids non-specifically, suggesting that CoV N

protein is an RNA chaperone (*8*). N is part of the replication/transcription complex and plays an important role in genomic replication, but its role in gene transcription is debated (*8-11*). N binds directly to cyclophilin (*12*) and hnRNP A1 (*13*). N protein has also been shown to mediate alterations in host cell processes to create a favorable environment for viral replication and production. N protein induces actin reorganization and apoptosis (*14*) and upregulates the AP1 pathway (*15*). N protein has also been shown to bind to the cyclin-dependent kinase complex and promote cell cycle arrest at the S phase (*16*).

The functional importance of a protein can be determined by abrogation at the gene, transcript, and protein levels. Gene knockouts and RNA interference techniques are powerful tools for assessing protein function. However, these methods have drawbacks. Both RNAi and gene knockout experiments are not specific to particular protein domains or protein function. Also, RNAi is often not completely effective in reducing function and may be inadequate when protein turnover is very slow. In order to directly assess functions specific to a domain, protein and small molecule affinity reagents that inhibit *in vivo* are informative (*17*).

With the creation of infectious cDNAs, reverse genetics of coronaviruses has helped demonstrate the essential functions of N protein early in the virus life cycle (*9, 11, 18*). However, N protein remains associated with viral RNA in the initial stages of viral integration (*19*), and it is not clear what if any contribution the associated N protein makes towards viral replication and host-cell interactions (*9, 14*). Therefore, direct inhibition at the protein level could be a complimentary method to assess the variety of N protein functions after infection with live virus. Also, domain specific inhibition may be

useful in assessing the contribution of different domains of N protein to modulation of various viral and cellular processes.

In vitro selection techniques such as phage display, ribosome display, and mRNA display have become standard tools for the generation of novel affinity reagents (*20*). While antibodies have been engineered to function intracellularly (*21, 22*), the reducing environment results in a reduction in stability which decreases the chances of obtaining functional inhibitors. Alternative scaffolds that function in the intracellular environment have been developed to overcome the limitation of expressing antibodies *in vivo* (*23, 24*). The Designed Ankyrin Repeat library developed by Pluckthun and colleagues has demonstrated superior expression characteristics (*25*). Using ribosome display, this library has generated intracellular inhibitors to a bacterial kinase (*26*), MAP kinase binders (*27*), and tobacco etch virus proteinase inhibitors (*28*).

The tenth fibronectin type III domain of human fibronectin (10FnIII), which is topologically analogous to the immunoglobulin VH domain, has been used as a scaffold for libraries for selection by phage display and mRNA display. The 10FnIII domain is an exceptionally stable domain that also expresses well in cells (*29*). Koide and colleagues first used a library based on 10FnIII to generate binders with modest affinities to ubiquitin (*30*), the estrogen receptor (*31*), and the SH3 domain (*32*). This domain was subsequently used for higher complexity libraries for use with mRNA display, resulting in binders to TNF-α and the vascular endothelial growth factor receptor 2 with affinities in the picomolar range after subsequent affinity maturation (*33, 34*).

In this study, we describe a fibronectin-based selection using mRNA display for protein affinity reagents that are specific to SARS N protein. The selection yielded

molecules that bind to either the NTD or CTD of N. Using surface plasmon resonance (SPR), we determined the affinity constant of the final pool winner, a CTD binder, and also a potent inhibitor which requires the NTD for binding. These molecules have affinities of 1.7 nM and 72 nM, respectively, demonstrating that high affinity binders are obtainable with only six rounds of selection without affinity maturation evolution. We demonstrated functionality both *in vitro* and *in vivo* and illustrate the potential for these molecules as tools for assessing N protein function *in vivo*.

Results

mRNA display selection

For mRNA display selection, the purity and functionality of the immobilized target protein is critical. Although N protein can be produce at high levels in bacteria, it has been demonstrated that N produced in eukaryotic cells is more immunogenic, at least partly due to its high level of phosphorylation (*35*). The recombinant N protein was engineered with an N-terminal $(His)_6$-tag and an N-terminal biotinylation signal peptide for *in vitro* biotinylation. The specific biotinylation scheme allows directional immobilization on streptavidin or neutravidin via only one N-terminal lysine, which may have advantages over other non-specific immobilization schemes. We assessed the functionality of the immobilized N protein by its ability to bind free N protein and M protein (data not shown).

For this selection, we used the scaffolded library described by Olson and Roberts (*29*). The domain is illustrated in Figure 4.1A. The library used for this selection began with greater than one trillion unique sequences. Briefly, each selection cycle includes

PCR, *in vitro* transcription, splint mediated ligation of the poly-dA-puromycin linker, urea PAGE purification, translation with fusion formation, oligo-dT cellulose purification, and reverse transcription. After the first round of selection, a FLAG-tag based preselection step was added to remove mRNA that was not fused to protein in order to increase the rate of enrichment. Also, we performed a pre-clear step to remove binders to the avidin-matrix beads by incubating the library with beads in batch 3 times. The reverse transcribed, purified fusions were then subjected to the selective enrichment of binders by binding immobilized N protein. We monitored enrichment for target specific binders by performing a radiolabeled pull-down assay (Figure 4.1B). Pool 3 was tested to monitor the prevention of selecting matrix binders over target binders. Initially, selection binding and washing was performed at 4ºC. After finding target specific enrichment at round 5, we increased the stringency of the selection and performed round 6 at physiological 37ºC. Pool 6 binding was very efficient, with greater than 60% of the pool remaining bound at 4ºC and 30% binding at physiological temperatures.

Pool 6 was cloned, and eighteen sequences were obtained. Nine representative binders were chosen for functional analysis (Figure 4.1C, D). Of the 18 sequences obtained, Fn-N22 and five clones with minor sequence variations comprise one third of the pool, while the remaining sequences were not found more than twice. The distribution of sequences in this pool demonstrates that a dominant binder, Fn-N22 and related sequences, was found, while a large amount of diversity still exists which increases the likelihood of obtaining molecules with distinct and beneficial properties. Also, each of the N binders obtained have highly dissimilar sequences, suggesting that each of these molecules may recognize N in a unique manner (Figure 4.1D). The binding analysis

demonstrates that Fn-N22 has the best pull-down efficiency as expected (68%), with little background binding to beads only. Other binders with high pull-down efficiency (57%-30%) include Fn-N10, Fn-N20, Fn-N15, Fn-N17, and Fn-N11. Two binders, Fn-N06 and Fn-N08, had lower efficiency of binding. One binder, Fn-N01 had relatively high background binding and poor target binding and was not characterized further.

Expression and binding validation

The fibronectin scaffolded library has an advantage over antibodies in that selected binders can be expressed in high levels in bacteria. In order to determine the ability of our N protein binders to express solubly in bacteria and retain function, we cloned the eight binders into a modified pET11 vector which adds a C-terminal $(His)_6$-tag. Fn-N06, Fn-N08, Fn-N10, Fn-N11, Fn-N15, Fn-N17, Fn-N20, and Fn-N22 were purified by nickel affinity chromatography from bacteria lysate and were used to pull-down pTAG-N protein from the transfected mammalian cell lysate. While expression levels varied greatly (Figure 4.2A, bottom panel), all 8 binders were able to pull-down mammalian N protein, with Fn-N10 and Fn-N22 being exceptionally efficient (Figure 4.2A, top panel). This pull-down was qualitatively similar to the immobilized N pull-down of *in vitro* expressed fibronectins (Figure 4.1C), with the exception of Fn-N15 being less efficient than expected.

We next determined the ability for the N binders to function in mammalian cells. The eight binders were cloned into a modified pIRES-puro vector that adds a FLAG-tag at the C-terminus. The binders were co-expressed with N protein and immunoprecipitated with anti-FLAG beads (Figure 4.2B). All eight binders express *in vivo*, and although

expression levels vary, all binders were immunoprecipitated efficiently. We detected co-immunoprecipitation (co-IP) of N protein with Fn-N10, Fn-N17, and Fn-N20 reproducibly.

We produced N truncation variants to map which domain that each fibronectin recognizes. The full-length N (N-WT), an N-terminal deletion mutant (N-ΔNTD), and the C-terminal domain (N-CTD) were purified from 293T cells (Figure 4.2C) and immobilized. Of the 8 binders tested, Fn-N17 and Fn-N20 could be precipitated by the full-length N protein only, indicating that these 2 binders require the RNA-binding NTD for binding. The other 6 fibronectins could bind all 3 N protein variants, indicating that they interact with the C-terminal self-association domain (Figure 4.2D). It is interesting to note that the pull-down efficiencies of the 6 C-terminal domain-specific binders are greater with constructs lacking the N-terminal domain. Of the CTD binders, Fn-N10 binds full-length N the best, which may explain why it is able to co-IP with N, while the other CTD binders do not (Figure 4.2B).

ELISA was used to compare the binding property of fibronectins to the commercially available antibodies (Figure 4.2E). His-tagged Fn-N17 and Fn-N20 were purified from bacteria using nickel affinity purification. The antibodies used were monoclonal anti-N protein antibody and anti-flag antibodies to target a flag epitope on the N protein. Both fibronectins capture N protein from the transfected cell lysate more efficiently than the antibodies at various antigen concentrations. At lower antigen concentration, the difference between the fibronectins and antibodies are less obvious; this could be due to the limit of detection in ELISA.

Fluorescence microscopy

The specific interaction between N-binding fibronectins and N protein was also demonstrated by co-localization using immunofluorescence microscopy. The co-localization of Fn-N10, Fn-N17, and Fn-N20 with N from SARS-CoV is demonstrated in Figure 4.3. The mammalian cell expression of each fibronectin was diffuse throughout the cytoplasm and the nucleus, represented by Fn-N10 in Figure 4.3. In infected cells, the fibronectin molecules are not found in the nucleus and are localized with viral N protein in the cytoplasm. The images show that N protein is able to recruit the fibronectin to the cytoplasm, particularly where N protein is found at higher density. Cells co-transfected with the fibronectins and N cDNA also demonstrate co-localization (data not shown).

Binding affinity

We chose two representative N-binding fibronectins to test the binding affinities achieved with this selection using surface plasmon resonance (SPR) (Figure 4.4). We expressed and purified Fn-N22, a CTD binder, and Fn-N17, an NTD-dependent binder for affinity determination. SARS N protein was prepped and purified as described for selection target preparation. N-terminal specific biotinylation allows for stable immobilization on a biacore streptavidin chip in a consistent manner. For Fn-N22, the selection winner, the association rate constant was 2.17 10^7 M^{-1} s^{-1} and the dissociation rate constant was 0.037 s^{-1}, resulting in an equilibrium dissociation constant of 1.7 nM. For Fn-N17, the association rate constant was 8.71 10^5 M^{-1} s^{-1} and the dissociation rate constant was 0.062 s^{-1}, resulting in an equilibrium dissociation constant of 72 nM (χ^2 = 0.3 RU^2 for both fits).

The relative affinities correspond to the relative *in vitro* pull-down efficiencies (68% vs. 30%).

Inhibition of SARS replication

After demonstrating *in vivo* expression and N protein binding by the selected fibronectins, assays were performed to examine the inhibition of viral replication by looking at viral gene expression. For higher infection efficiency, a stable 293T cell line expressing SARS-CoV receptor ACE2 (293T-ACE2) was used. After transient transfection of N-binding fibronectins, viral gene expression was assayed by measuring *Renilla* luciferase activity in SARS-CoV/RL-infected producer cells (Figure 4.5A). In the SARS-CoV/RL variant, ORF7 is replaced with the *Renilla* luciferase gene. Replication of this mutant virus is not affected compared to wild type SARS-CoV. The fold inhibition of gene expression was defined as the ratio of luciferase activity from plasmid only versus fibronectin-expressing cells. Fn38 was used as a target non-specific control that was randomly derived from the naïve fibronectin library (*29*). As an additional control to rule out the possibility of non-specific inhibition by fibronectin overexpression, a similar assay was performed with firefly luciferase expressing murine γ-Herpesvirus 68(MHV-68/M3Luc). In the MHV-68/M3Luc reporter virus, the non-essential M3 gene is replaced by the firefly luciferase gene, which does not effect replication. Of the 8 binders tested, only Fn-N08 demonstrated significant background inhibition of MHV-68/M3Luc production (8-fold, data not shown). Thus, Fn-N08 was excluded from the subsequent viral inhibition assays as its inhibitory effect might not be virus specific. All other N-binding fibronectins did not inhibit MHV-68/M3Luc replication significantly, indicating

that inhibition of SARS-CoV replication is not due to the adverse effect of binder expression alone (data not shown).

Fn-N10 demonstrates the strongest inhibition of viral gene transcription during infection, approximately 29-fold over the plasmid only control, followed by the Fn-N22 and Fn-N17, which inhibit 7- and 5-fold, respectively (figure 5A). Other binders reduce viral gene transcription only up to 2-fold, while the non-specific control Fn38 has no effect. The luciferase assay was performed 20 hours post-infection. To examine the effect of N-binding fibronectins on SARS-CoV replication more closely, inhibition dose curves were done. Four binders tested inhibit viral gene expression in a dose dependent manner (data not shown).

Since many N-binding fibronectins inhibit SARS-CoV replication, additional studies were performed to investigate which step of viral replication is affected. Inhibition of viral gene transcription, specifically the ORF N subgenomic mRNA, was quantitated by real time qPCR (Figure 4.5B). After normalizing to actin transcription, Fn-N10 inhibits viral gene transcription by approximately 13-fold compared to the backbone plasmid control. Fn-N20 and Fn-N22 inhibit approximately 3-fold, while Fn-N15 and Fn-N17 do not inhibit more than the control Fn38.

Inhibition of viral production

We further examined inhibition of SARS replication by measuring viral production (Figure 4.6). We correlated inhibition of virus production by expanding virus obtained from cells expressing fibronectin N-inhibitors in new cells and subsequently measuring luciferase activity. To examine whether the *Renilla* luciferase activity can be directly

correlated to the amount of virions in the supernatant, a titration of viral infection was done. At 16hr post infection with MOI 0.1 to MOI 6.4, the luciferase activity has a linear correlation to MOI (Figure 4.6A). The strongest inhibitor, Fn-N10, reduces virus production by greater than 3 logs (Figure 4.6B). Fn-N22 inhibits virus production approximately 600-fold. All other fibronectins inhibit between 10- to 60-fold while control Fn-38 again has a negligible effect. The inhibition of viral production was dose-dependent (data not shown).

We also tested the ability for fibronectins that recognize non-overlapping epitopes to inhibit virus production synergistically. Fn-N17, Fn-N20, and Fn-N22 were transfected into cells at sub-optimal concentration (Figure 4.6C). At this concentration, expression of Fn-N17, Fn-N20, and Fn-N22 alone inhibit viral production 4-, 2-, and 6.6-fold, respectively. Expression of Fn-N17 with Fn-N20 together only has an additive effect on virus inhibition. However, co-expressing Fn-N17 with Fn-N22 or Fn-N20 with Fn-N22 dramatically increases the inhibition to greater than 100-fold; thus, both combinations inhibit synergistically.

Discussion

mRNA-display has successfully been utilized to select high affinity protein reagents that differentially target a SARS-CoV viral protein, N. After 6 rounds, we sequenced a fraction of the resulting pool and analyzed it for highly functional proteins. A family of sequences was found at a high frequency (6 of 18) and had highest binding efficiency (68% *in vitro*), indicating the pool was converging to a selection winner. This pool still contained much diversity, however, which allowed us to assay a number of unique

fibronectin molecules. Each binder is unique in sequence, indicating that each represents a separate solution to N protein recognition. Each sequence contains a high representation of aromatic and polar residues, typical of protein interactions surfaces. Basic residues are found while acid residues are rare, indicating that the binders do not simply recognize the basic nucleic acid binding regions of N.

The fibronectins were functional and able to be expressed in a number of formats. In addition to the reticulocyte lysate expression system, fibronectins were well-expressed in bacteria and mammalian cells, including 293T and VERO cells. Binding was demonstrated by pull-down, co-IP, and IFA. ELISA was also used to demonstrate that two of the binders have equal or better function relative to a monoclonal antibody. Six of 8 N-binding fibronectins tested are able to bind to the CTD alone, while 2 require the NTD for binding. One CTD binder and one NTD-dependent binder were analyzed for affinity. Fn-N22 and Fn-N17 bind to N protein with high affinity, similar to monoclonal antibodies (Kd = 1.7 nM and Kd=71 nM respectively). Further affinity maturation evolution may be performed to improve these affinities and would improve the potential of these binders for ultra-sensitive detection platforms.

Four of the fibronectins demonstrate significant inhibition of SARS-CoV replication when transiently expressed in mammalian cell culture. Fn-N10 and Fn-N22 both bind to the N-CTD and have a larger effect on inhibition compared to the NTD-dependent binders Fn-N17 and Fn-N20. Fn-N10 inhibits viral gene expression and virus production the greatest. It is also interesting to note that while Fn-N22 has the highest pull-down efficiency by immobilized N protein, it is not able to co-IP with N protein, while Fn-N10 does efficiently co-IP. The differences in inhibition may lie in the ability

for the two proteins to recognize different conformations of N. Fn-N10 is able to recognize the full-length N protein much more efficiently compared to Fn-N22, while both proteins efficiently recognize the CTD alone (Figure 4.2D).

The two fibronectins which require the N NTD for binding, Fn-N17 and Fn-N20, also inhibit SARS replication, though less efficiently than Fn-N10 and Fn-N22. The NTD is thought to mediate binding to the genomic RNA essential for the formation of ribonucleoprotein complex (*2*). One potential reason for observing a smaller inhibitory effect at the NTD may be due to a lower functional impact of the N-NTD in SARS replication relative to the CTD. Further analysis may determine specific contributions for each domain in specific aspects of SARS replication.

Due to the differential recognition of the N-binding fibronectins, we sought to demonstrate cooperative inhibition of virus replication. While Fn-N17 and Fn-N20 display only additive inhibition of viral production when co-expressed, both demonstrate a synergistic effect when each is co-expressed with Fn-N22 (figure 4.6B). Common antiviral therapeutic strategies employ drug cocktails which target multiple aspects of viral replication. Our data demonstrates the value of this strategy with respect to SARS. An interesting point is that cooperative inhibition was achieved by targeting multiple domains of a single multifunctional protein. Also, most antiviral therapeutics strategies center on the targeting of enzymatic function. This study demonstrates the efficacy of targeting a structural protein if small molecules could be developed to disrupt N protein function in a similar manner. The large amount of inhibition in virus production achieved by the fibronectins might indicate that the interruption of virus capsid formation can be a particularly effective antiviral strategy.

This study demonstrates the utility of mRNA display selections for fibronectin-based intracellular inhibitors. The fibronectin scaffold provides a suitable platform for the generation of intracellular inhibitors that have advantages over conventional intracellular antibodies known as "intrabodies" (*17*). Fibronectin molecules are able to be expressed in bacteria for biophysical characterization and are stable in mammalian cell culture. No *in vivo* screen was required to filter the resulting pool for binders that function inside the cell.

Direct knock-down of protein function is a complimentary tool for the analysis of proteins *in vivo* in addition to standard genetic tools. The fibronectin inhibitors introduced in this study could be used for further analysis or conformation of N protein's function in viral replication using unmodified SARS virus. The N-binding fibronectins could also be informative for investigating how N protein interacts with host cell proteins during various stages of the virus life cycle. For this application, direct protein knock-down would enable correlation of host cell interactions to N protein function using wild type virus under native conditions. The selected fibronectins also have potential for *in vivo* visualization. We demonstrated that the N-binding fibronectins are able to co-localize to N protein produced by wild type SARS-CoV. These molecules could be used to analyze the fate of N and the ribonucleoprotein complex in real time during initial stages of virus entry. The versatility of the fibronectin scaffold and the selection technique will enable the generation of functional intracellular affinity reagents for any number of applications.

Experimental Procedures:

Cell culture

293T, 293T-ACE2, and VERO cells were cultured in DMEM (Dulbecco's modified Eagle's medium) containing 10% FBS. The wild type SARS-CoV Urbani strain was obtained from the CDC. The SARS-CoV *Renilla* Luciferase mutant was a gift from Ralph S Baric. Both viruses were propagated in VERO cells. The Murine γ-Herpesvirus 68-luciferase virus (MHV-68/M3FL) was constructed by inserting the viral M3 promoter-driven firefly luciferase cassette between genomic coordinates 746 and 747 of MHV-68 (U97553).

Plasmids

SARS-CoV N was first amplified from cDNA derived from WT SARS-CoV infected VERO cells with Nf-BtsI (5'-GGA AGG CAG TGA TGT CTG ATA ATG GAC CCC AAT) and Nf-BamHI (5'-CGG GAT CCT TAT GCC TGA GTT GAA TCA GCA). The PCR product was digested with BstI and BamHI (NEB) and ligated into pDW363C, which was digested with BseRI and BamHI (*36*). N was subcloned from pDW363C-N into pcDNA3 for mammalian expression using NpcDNAF (5'-A AGG TAC CGC CAC C ATG CAC CAC CAT CAC CAT CAC GC TGG AGG CCT GAA CGA TAT) and NpcDNAR (5'-TAG GGC CCT TAT GCC TGA GTT GAA TCA GCA G) using KpnI ApaI restriction sites. The N-ΔNTD and N-CTD fragments were subcloned from pcDNA3-N using primers N-ΔNTDF (5'-CTG GAG GCA TCG AGG GTC GC C AAG CCT CTT CTC GCT CCT C) and N-CTDF (5'-CTG GAG GCA TCG AGG GTC GC A

CTA AGA AAT CTG CTG CTG A). pTAG-N was cloned separately and provided by Nikki Reyes.

The fibronectin PCR product from pool 6D was cloned into pCR4-TOPO (Invitrogen) for sequencing. For bacterial expression, selected fibronectins were further subcloned into the NdeI and BamHI restriction sites of pAO5 (see appendix A) using Fnlibrary5NdeI (5'-CTA TTT ACA ATT CAT ATG CTC GAG GTC GTC G) and Fnoligo8 (5'-GGA GCC GCT ACC GGA TCC GGT GCG GTA GTT GAT GGA GAT CGG). For expression in mammalian cell culture, fibronectins were amplified with Fn5pIRES (5'-CTT CTA GCG GCC GCC ACC ATG CTC GAG GTC GTC G) and Fn3FLAG (5'-GTG ACC TGA TCA CTT ATC GTC GTC ATC CTT GTA ATC GGA TCC GGT GCG GTA GTT GAT GGA GAT CG). The PCR products were digested with NotI and BclI and ligated into the NotI and BamHI restriction sites of pIRESpuro (Clontech), creating C-terminal Flag-tagged proteins.

N protein purification

In order to produce the biotinylated N target, 293T cells were seeded into 10 cm plates and transfected with pcDNA3-N using Lipofectamine Plus per the manufacturer's recommendation (Invitrogen). N protein was harvested with RIPA buffer at 30 hours post transfection, purified from cleared cell lysates with Nickel-NTA beads (Qiagen), buffer exchanged with Nap-5 columns, (Amersham Biosciences), biotinylated by biotin ligase (Avidity), desalted with Nap-5 columns, and conjugated to streptavidin acrylamide or neutravidin agarose beads (Pierce).

mRNA display

For the first round of selection, approximately one trillion unique library DNA molecules were amplified by PCR using Fnoligo1 (5'-TTC TAA TAC GAC TCA CTA TAG GGA CAA TTA CTA TTT ACA ATT ACA ATG CTC GAG GTC GTC G) and Fnoligo8 (see above). For each round of selection, the PCR product was transcribed by *in vitro* runoff transcription with T7 RNA polymerase. Library RNA was ligated with T4 DNA ligase (NEB) to a DNA linker which contains puromycin at the 3' end (pF30P: 5'-phospho-A_{21}-9_3-ACC-Pu, 9 = phosphoramidite spacer 9, Pu = Puromycin, Glen Research). Ligation was mediated by a splint complimentary to the 3' library and 5' linker sequences (Fn-pF30P-Splint: 5'-TTTTTTTTTTTTGGAGCCGCTACC). Ligated library mRNA was purified by urea PAGE and translated *in vitro* with rabbit reticulocyte lysate (Red NOVA, Novagen). Fusion formation was enhanced by addition of potassium and magnesium as described (*37*). RNA-fibronectin fusions were purified with oligo-dT cellulose beads (NEB) and desalted following elution (Centri-sep, Princeton Separations). The fusions were reverse transcribed (Superscript II, Invitrogen) prior to affinity enrichment with immobilized N protein. Binding and washing buffer contained PBS plus 0.02% Tween 20, 0.5 mg/ml BSA (Sigma), and 0.1 mg/ml sheared salmon sperm DNA (Sigma). After the first round of selection, the enriched DNA pool was amplified by Fnoligo9, which adds a Flag tag sequence to the 3' end of the fibronectin pool (Fnoligo9: 5'- GGA GCC GCT ACC CTT ATC GTC GTC ATC CTT GTA ATC GGA TCC GGT GCG GTA GTT GAT GGA GAT CG) . Fnoligo10 was used for subsequent fibronectin pool amplifications and reverse transcriptions (Fnoligo10: 5'-GGA GCC GCT ACC CTT ATC GTC G). After round one, fusion pools were subjected to flag tag purification with

anti-flag M2 agarose beads (Sigma) and were eluted with 3XFLAG peptide (Sigma). Rounds 2 – 6 also included a negative selection step to remove background binders by incubation with empty beads in batch 3 times. Binding and washing was performed at 4ºC for rounds 1 – 5 and at 37ºC for round 6.

In vitro binding assay

Radiolabelled fusions were prepared and purified with oligo-dT cellulose beads as described for the selection, except translation reactions were performed in buffer lacking Methionine and were supplemented with L-[^{35}S]Methione (MP Biomedicals). Fusion pools were incubated with ribonuclease A (Roche) prior to measuring binding efficiencies. Individual pool 6 clones were amplified from pCR4-TOPO with Fnoligo1 and Fnoligo9 (see above). Following in vitro transcription, the RNA products were phenol-chloroform extracted, ethanol precipitated, and desalted with centri-sep spin columns (Princeton Separations). Purified RNA was *in vitro* translation with rabbit reticulocyte lysate (Red Nova, Novagen) in the presence of L-[^{35}S]Methionine. Fibronectin proteins were then flag-tag purified with anti-flag M2 agarose beads (Sigma) using 3XFLAG peptide for elution. Radiolabeled fibronectin pools and individual pool 6 N-binding fibronectins were incubated with immobilized N protein or empty beads. After washing in selection buffer, binding efficiencies were determined by scintillation counting. Pool binding assays were performed at either 4ºC or 37ºC, as indicated. Individual fibronectin bindings were performed at room temperature.

N pull-down

For bacteria expression, *E. Coli* BL21 (DE3) were chemically transformed with pAO5 containing N-binding fibronectin clones. Protein expression was induced at mid log phase (OD ~ 0.4) with 1 mM IPTG for 3 hours at 37°C. Cells were lysed by sonication and fibronectins were immobilized on nickel-NTA beads (Qiagen). 293T cells were transfected with pTAG-N using Lipofectamine Plus (Invitrogen) and were lysed with incomplete RIPA buffer (10 mM Tris pH 8.0, 1% NP-40, 150 mM NaCl). Cleared cell lysate was incubated with immobilized fibronectin or blank beads as a control. After washing in modified RIPA buffer, the precipitated proteins were eluted and separated by SDS-PAGE. Proteins were transferred to nitrocellulose (Schleicher & Schuell) and developed with ECL Western Blotting Detection Kit (Amersham Biosciences). Fibronectins were detected by coomassie stain, and N was detected with mouse anti-SARS-Nucleoprotein (Zymed).

Co-immunoprecipitation

293T cells were co-transfected with pcDNA3-N and each pIRES-fibronectin binder with Lipofectamine Plus. Cells were harvested 30 hours post-transfection with incomplete RIPA buffer (10 mM Tris pH 8.0, 1% NP-40, 150 mM NaCl, 1 mM EDTA). Cell lysates were incubated overnight at 4°C with protein G sepharose beads (Amersham Biosciences) conjugated with anti-flag antibody (Sigma). The precipitants were washed 4 times with RIPA buffer, once with PBS, and separated by SDS-PAGE for western blot analysis. N was detected with mouse anti-SARS-Nucleoprotein (Zymed), and fibronectins were detected using mouse anti-flag antibody (Sigma).

Domain mapping by pull-down

pcDNA3 containing N-WT, N-ΔNTD, and N-CTD were transfected into 293T cells and immobilized with nickel-NTA beads. The immobilized proteins were analyzed by SDS-PAGE using coomossie stain. 293T cells expressing each fibronectin were lysed, and cleared lysate was incubated with immobilized N fragments overnight at 4°C. The pull-downs were washed 4 times with RIPA buffer and analyzed by western blot.

ELISA

Nickel affinity purified fibronectins, monoclonal anti-SARS N protein antibody (Zymed), and anti-flag antibody (Sigma) were used to coat 96 well Nunc-immuno plates (Nunc) in 50 μl of 50 mM carbonate bicarbonate buffer (Sigma) over night at 4°C. The plates were blocked with 2% BSA in PBST for 1 hour. The antigen-containing cell lysate was diluted in PBST. Untransfected 293T cells and 293T cells transfected with pTAG-N were harvested with RIPA buffer. Cell lysates were diluted in PBST and incubated with immobilized antibodies or fibronectins for one hour. After washing, wells were incubated with polyclonal anti-SARS N protein antibody (Imagnex), followed by incubation with anti-rabbit HRP conjugated antibody. The plates were developed with SIGMA FAST OPD tablet (Sigma), and reactions were stopped with 4N H_2SO_3 (Sigma) and analyzed

Immunofluorescence microscopy

VERO cells were seeded in 8-well chamber slides and transfected with pIRES-fibronectins. Transfected cells were infected with wild type SARS-CoV at MOI 0.1 24 hours post transfection. At 16hr post infection, the cells were fixed with 2%

paraformaldehyde for a minimum of 40 min before washing with PBS. Antibody incubations were done following standard protocols. Fibronectins were detected by anti-flag antibody (Sigma) and Alexa Fluor 488 goat anti-mouse IgG (Invitrogen). N protein was detected by polyclonal anti-SARS N protein antibody (Imgenex) and goat anti-rabbit Cy3 conjugated antibody (Invitrogen). Images were taken with a Leica fluorescence microscope equipped with a CCD camera using the appropriate filters.

Surface plasmon resonance

Binding kinetics were obtained with a Biacore T100 instrument using a streptavidin sensor chip. Biotinylated N protein was prepared as described above and loaded at a density of 800 RU. Fn-N17 and Fn-N22 were expressed in *E. coli* BL21(DE3) and purified by nickel affinity chromatography and ion exchange chromatography (Amersham Biosciences). Various concentrations of either Fn-N17 or Fn-N22 were flowed over a blank streptavidin chip and the N-coated chip at 100 μl per minute for 120 seconds, and were allowed to fall off for one hour. Kinetic data were obtained by fitting with the Biacore evaluation software.

Luciferase assays

293T cells were seeded, transfected with fibronectin inhibitors as indicated, and infected with the SARS-CoV *Renilla* Luciferase strain. Cell supernatants were collected from the primary transfected and infected cells 16 hours post infection and were used to infect fresh 293T-ACE2 cells seeded in 384 well plates. The primary cells were also harvested to measure inhibition of luciferase expression. The secondary destination cells were

collected 20 hours post infection to determine the relative inhibition of virus production. Both primary and secondary cells were harvested with Passive Lysis Buffer for analysis by the *Renilla* Luciferase Assay System (Promega) or Dual Luciferase Reporter Assay System (Promega).

Quantitative PCR

293T-ACE2 cells were transfected with pIRES-fibronectins and infected with wild type SARS-CoV. Total infected cell RNA was extracted first by TRI-reagent (Invitrogen) and was further purified with the Micro-to-midi RNA purification system (Invitrogen). cDNAs were created with Superscript III (Invitrogen) using random hexomers. Viral N gene transcripts were amplified using primers SARS/qPCR-NF (5'-GGA GCC TTG AAT ACA CCC AAA G) and SARS/qPCR-NR (5'-GCA CGG TGG CAG CAT TG) following the standard SYBR green quantitative PCR protocol. Standards to calculate copy number were derived by TOPO-TA cloning amplified PCR product into pCR4-TOPO. Quantitative PCR was performed with human beta-actin cDNA as a normalization control for each sample using primers ACTB-5F (5'-CAC CCA CAC TGTG CCC ATC TAC) and ACTB-3R (5'-GTG AGG ATC TTC ATG AGG TAG TC).

References

(1) Rota, P. A., Oberste, M. S., Monroe, S. S., Nix, W. A., Campagnoli, R., Icenogle, J. P., Penaranda, S., Bankamp, B., Maher, K., Chen, M. H., Tong, S., Tamin, A., Lowe, L., Frace, M., DeRisi, J. L., Chen, Q., Wang, D., Erdman, D. D., Peret, T. C., Burns, C., Ksiazek, T. G., Rollin, P. E., Sanchez, A., Liffick, S., Holloway, B., Limor, J., McCaustland, K., Olsen-Rasmussen, M., Fouchier, R., Gunther, S., Osterhaus, A. D., Drosten, C., Pallansch, M. A., Anderson, L. J., and Bellini, W. J. (2003) Characterization of a novel coronavirus associated with severe acute respiratory syndrome. *Science 300*, 1394-9.

(2) Saikatendu, K. S., Joseph, J. S., Subramanian, V., Neuman, B. W., Buchmeier, M. J., Stevens, R. C., and Kuhn, P. (2007) Ribonucleocapsid formation of severe acute respiratory syndrome coronavirus through molecular action of the N-terminal domain of N protein. *J Virol 81*, 3913-21.

(3) Surjit, M., Liu, B., Kumar, P., Chow, V. T., and Lal, S. K. (2004) The nucleocapsid protein of the SARS coronavirus is capable of self-association through a C-terminal 209 amino acid interaction domain. *Biochem Biophys Res Commun 317*, 1030-6.

(4) Chen, C. Y., Chang, C. K., Chang, Y. W., Sue, S. C., Bai, H. I., Riang, L., Hsiao, C. D., and Huang, T. H. (2007) Structure of the SARS coronavirus nucleocapsid protein RNA-binding dimerization domain suggests a mechanism for helical packaging of viral RNA. *J Mol Biol 368*, 1075-86.

(5) Satija, N., and Lal, S. K. (2007) The molecular biology of SARS coronavirus. *Ann N Y Acad Sci 1102*, 26-38.

(6) You, J., Dove, B. K., Enjuanes, L., DeDiego, M. L., Alvarez, E., Howell, G., Heinen, P., Zambon, M., and Hiscox, J. A. (2005) Subcellular localization of the severe acute respiratory syndrome coronavirus nucleocapsid protein. *J Gen Virol 86*, 3303-10.

(7) Surjit, M., Kumar, R., Mishra, R. N., Reddy, M. K., Chow, V. T., and Lal, S. K. (2005) The severe acute respiratory syndrome coronavirus nucleocapsid protein is

phosphorylated and localizes in the cytoplasm by 14-3-3-mediated translocation. *J Virol 79*, 11476-86.

(8) Zuniga, S., Sola, I., Moreno, J. L., Sabella, P., Plana-Duran, J., and Enjuanes, L. (2007) Coronavirus nucleocapsid protein is an RNA chaperone. *Virology 357*, 215-27.

(9) Schelle, B., Karl, N., Ludewig, B., Siddell, S. G., and Thiel, V. (2005) Selective replication of coronavirus genomes that express nucleocapsid protein. *J Virol 79*, 6620-30.

(10) Enjuanes, L., Almazan, F., Sola, I., Zuniga, S., Alvarez, E., Reguera, J., and Capiscol, C. (2006) Biochemical aspects of coronavirus replication. *Adv Exp Med Biol 581*, 13-24.

(11) Almazan, F., Galan, C., and Enjuanes, L. (2004) The nucleoprotein is required for efficient coronavirus genome replication. *J Virol 78*, 12683-8.

(12) Luo, C., Luo, H., Zheng, S., Gui, C., Yue, L., Yu, C., Sun, T., He, P., Chen, J., Shen, J., Luo, X., Li, Y., Liu, H., Bai, D., Yang, Y., Li, F., Zuo, J., Hilgenfeld, R., Pei, G., Chen, K., Shen, X., and Jiang, H. (2004) Nucleocapsid protein of SARS coronavirus tightly binds to human cyclophilin A. *Biochem Biophys Res Commun 321*, 557-65.

(13) Luo, H., Chen, Q., Chen, J., Chen, K., Shen, X., and Jiang, H. (2005) The nucleocapsid protein of SARS coronavirus has a high binding affinity to the human cellular heterogeneous nuclear ribonucleoprotein A1. *FEBS Lett 579*, 2623-8.

(14) Surjit, M., Liu, B., Jameel, S., Chow, V. T., and Lal, S. K. (2004) The SARS coronavirus nucleocapsid protein induces actin reorganization and apoptosis in COS-1 cells in the absence of growth factors. *Biochem J 383*, 13-8.

(15) He, R., Leeson, A., Andonov, A., Li, Y., Bastien, N., Cao, J., Osiowy, C., Dobie, F., Cutts, T., Ballantine, M., and Li, X. (2003) Activation of AP-1 signal transduction pathway by SARS coronavirus nucleocapsid protein. *Biochem Biophys Res Commun 311*, 870-6.

(16) Surjit, M., Liu, B., Chow, V. T., and Lal, S. K. (2006) The nucleocapsid protein of severe acute respiratory syndrome-coronavirus inhibits the activity of cyclin-

cyclin-dependent kinase complex and blocks S phase progression in mammalian cells. *J Biol Chem 281*, 10669-81.

(17) Stocks, M. (2005) Intrabodies as drug discovery tools and therapeutics. *Curr Opin Chem Biol 9*, 359-65.

(18) Yount, B., Curtis, K. M., Fritz, E. A., Hensley, L. E., Jahrling, P. B., Prentice, E., Denison, M. R., Geisbert, T. W., and Baric, R. S. (2003) Reverse genetics with a full-length infectious cDNA of severe acute respiratory syndrome coronavirus. *Proc Natl Acad Sci U S A 100*, 12995-3000.

(19) Ng, M. L., Tan, S. H., See, E. E., Ooi, E. E., and Ling, A. E. (2003) Early events of SARS coronavirus infection in vero cells. *J Med Virol 71*, 323-31.

(20) Lipovsek, D., and Pluckthun, A. (2004) In-vitro protein evolution by ribosome display and mRNA display. *J Immunol Methods 290*, 51-67.

(21) Tanaka, T., Lobato, M. N., and Rabbitts, T. H. (2003) Single domain intracellular antibodies: a minimal fragment for direct in vivo selection of antigen-specific intrabodies. *J Mol Biol 331*, 1109-20.

(22) der Maur, A. A., Zahnd, C., Fischer, F., Spinelli, S., Honegger, A., Cambillau, C., Escher, D., Pluckthun, A., and Barberis, A. (2002) Direct in vivo screening of intrabody libraries constructed on a highly stable single-chain framework. *J Biol Chem 277*, 45075-85.

(23) Hosse, R. J., Rothe, A., and Power, B. E. (2006) A new generation of protein display scaffolds for molecular recognition. *Protein Sci 15*, 14-27.

(24) Binz, H. K., and Pluckthun, A. (2005) Engineered proteins as specific binding reagents. *Curr Opin Biotechnol 16*, 459-69.

(25) Binz, H. K., Stumpp, M. T., Forrer, P., Amstutz, P., and Pluckthun, A. (2003) Designing repeat proteins: well-expressed, soluble and stable proteins from combinatorial libraries of consensus ankyrin repeat proteins. *J Mol Biol 332*, 489-503.

(26) Amstutz, P., Binz, H. K., Parizek, P., Stumpp, M. T., Kohl, A., Grutter, M. G., Forrer, P., and Pluckthun, A. (2005) Intracellular kinase inhibitors selected from combinatorial libraries of designed ankyrin repeat proteins. *J Biol Chem 280*, 24715-22.

(27) Amstutz, P., Koch, H., Binz, H. K., Deuber, S. A., and Pluckthun, A. (2006) Rapid selection of specific MAP kinase-binders from designed ankyrin repeat protein libraries. *Protein Eng Des Sel 19*, 219-29.

(28) Kawe, M., Forrer, P., Amstutz, P., and Pluckthun, A. (2006) Isolation of intracellular proteinase inhibitors derived from designed ankyrin repeat proteins by genetic screening. *J Biol Chem 281*, 40252-63.

(29) Olson, C. A., and Roberts, R. W. (2007) Design, expression, and stability of a diverse protein library based on the human fibronectin type III domain. *Protein Sci 16*, 476-84.

(30) Koide, A., Bailey, C. W., Huang, X., and Koide, S. (1998) The fibronectin type III domain as a scaffold for novel binding proteins. *J Mol Biol 284*, 1141-51.

(31) Koide, A., Abbatiello, S., Rothgery, L., and Koide, S. (2002) Probing protein conformational changes in living cells by using designer binding proteins: application to the estrogen receptor. *Proc Natl Acad Sci U S A 99*, 1253-8.

(32) Karatan, E., Merguerian, M., Han, Z., Scholle, M. D., Koide, S., and Kay, B. K. (2004) Molecular recognition properties of FN3 monobodies that bind the Src SH3 domain. *Chem Biol 11*, 835-44.

(33) Getmanova, E. V., Chen, Y., Bloom, L., Gokemeijer, J., Shamah, S., Warikoo, V., Wang, J., Ling, V., and Sun, L. (2006) Antagonists to human and mouse vascular endothelial growth factor receptor 2 generated by directed protein evolution in vitro. *Chem Biol 13*, 549-56.

(34) Xu, L., Aha, P., Gu, K., Kuimelis, R. G., Kurz, M., Lam, T., Lim, A. C., Liu, H., Lohse, P. A., Sun, L., Weng, S., Wagner, R. W., and Lipovsek, D. (2002) Directed evolution of high-affinity antibody mimics using mRNA display. *Chem Biol 9*, 933-42.

(35) Shin, G. C., Chung, Y. S., Kim, I. S., Cho, H. W., and Kang, C. (2007) Antigenic characterization of severe acute respiratory syndrome-coronavirus nucleocapsid protein expressed in insect cells: The effect of phosphorylation on immunoreactivity and specificity. *Virus Res 127*, 71-80.

(36) Ja, W. W., Adhikari, A., Austin, R. J., Sprang, S. R., and Roberts, R. W. (2005) A peptide core motif for binding to heterotrimeric G protein alpha subunits. *J Biol Chem 280*, 32057-60.

(37) Liu, R., Barrick, J. E., Szostak, J. W., and Roberts, R. W. (2000) Optimized synthesis of RNA-protein fusions for in vitro protein selection. *Methods Enzymol 318*, 268-93.

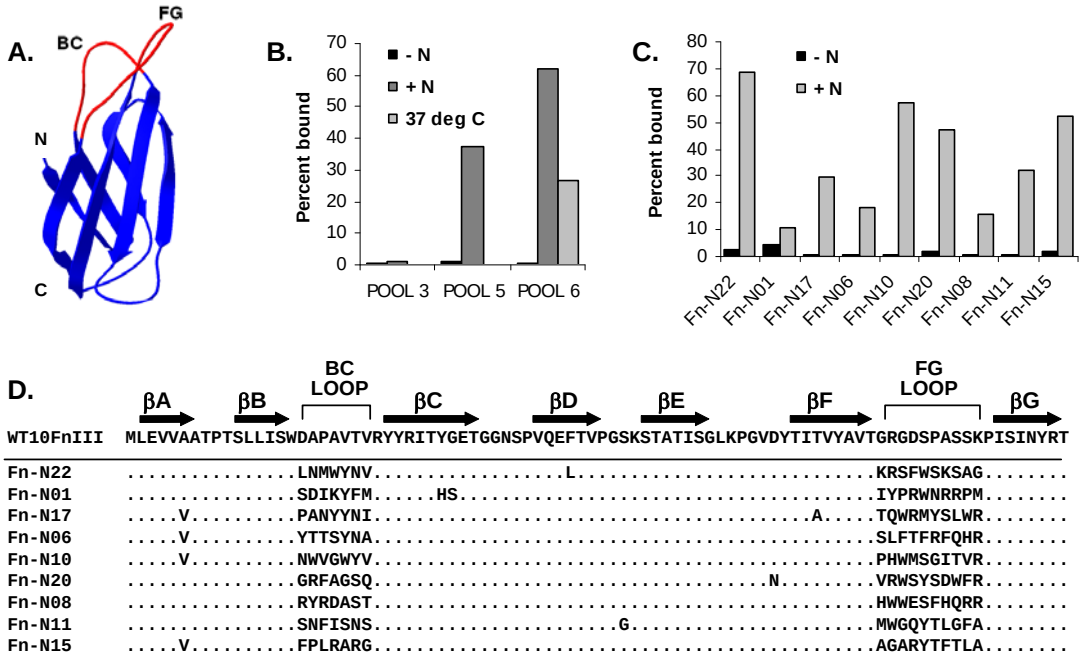

Figure 4.1 mRNA display selection of N binders using a 10FnIII scaffolded library. A.) An illustration of the 10FnIII solution structure using PDB file 1TTG, created with the Swiss PDB viewer. B) Radiolabeled fusion pool binding assay. C) Radiolabeled binding assay of Flag-tag purified N-binding fibronectins. D) Amino acid sequence of wild type 10FnIII and pool 6 binders. Dots represent residues identical to wild type 10FnIII.

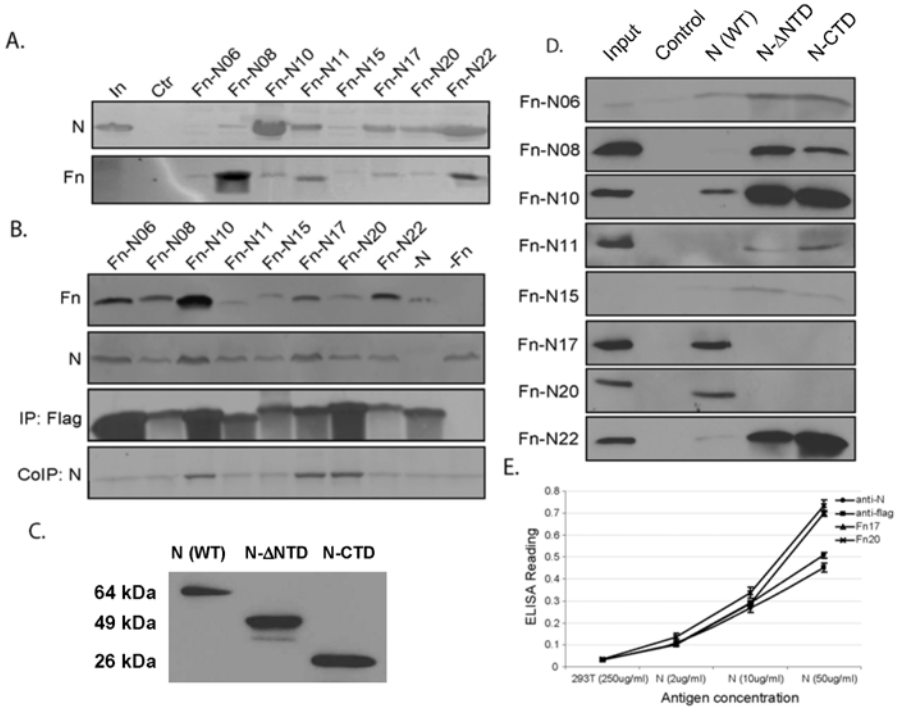

Figure 4.2 Expression of N-binding fibronectins that recognize multiple N domains. A) Bacterially expressed, $(His)_6$-tag purified fibronectins were used to pull-down transiently expressed N protein from 293T cells. B) Flag-tagged fibronectins and N protein were transiently co-expressed in 293T cells. Fibronectins were immobilized and were analyzed for the ability to co-precipitate N protein. C) Full-length N and two truncation mutants were expressed and purified via $(His)_6$-tags. D) Immobilized N fragments were used to pull-down flag-tagged fibronectins from transiently transfected 293T cells. E) ELISA was used to compare bacterially expressed, $(His)_6$-tag purified, N-binding fibronectins with a monoclonal anti-SARS antibody and anti-flag antibody.

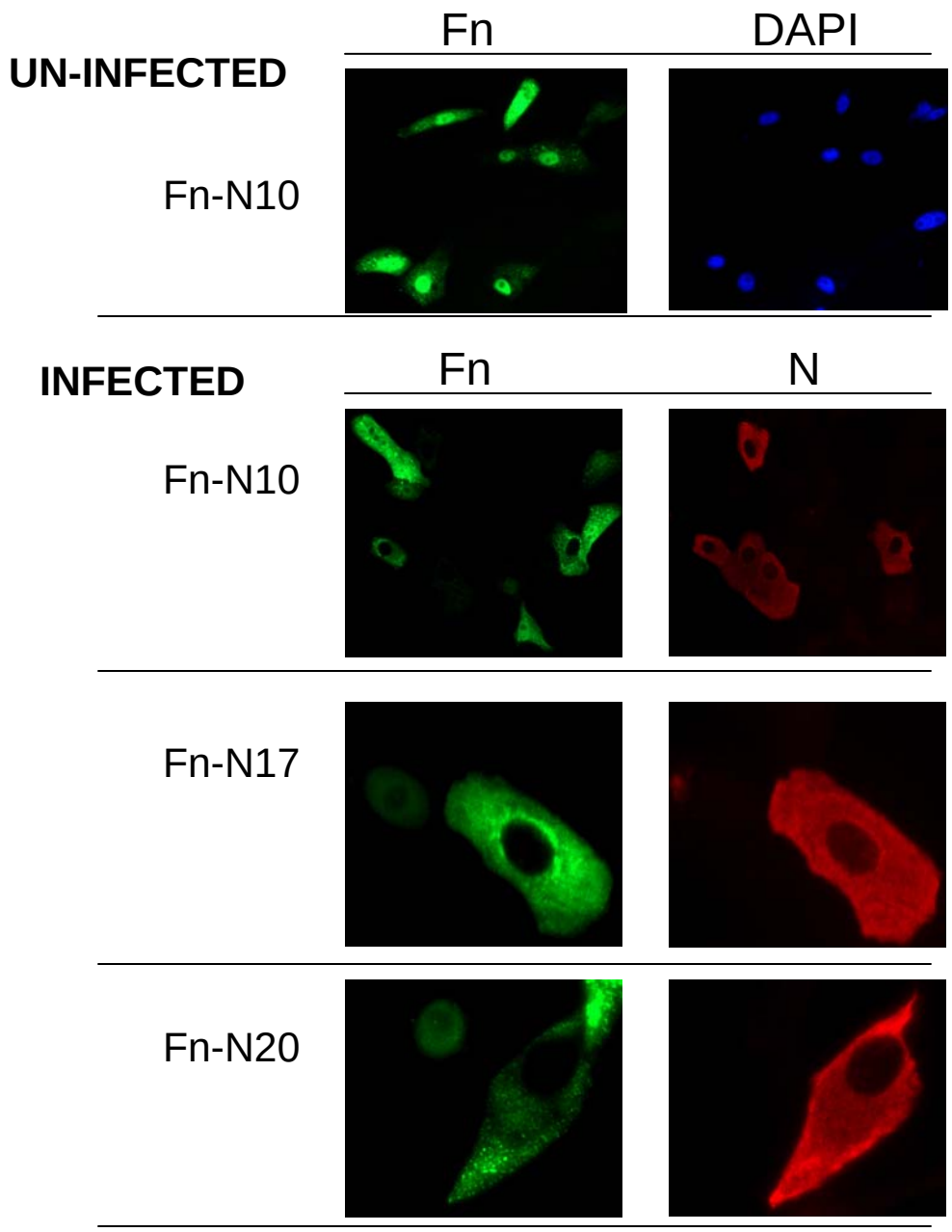

Figure 4.3 Immunofluorescence microscopy to demonstrate intracellular detection of N. Vero cells transiently transfected with fibronectins were infected with SARS-CoV and were fixed 16 hours post infection. Fibronectins were detected with mouse anti-flag antibody and Alexa Fluor 488 conjugated goat anti-mouse antibody. N was detected with rabbit anti-N antibody and Cy3 conjugated goat anti-rabbit antibody.

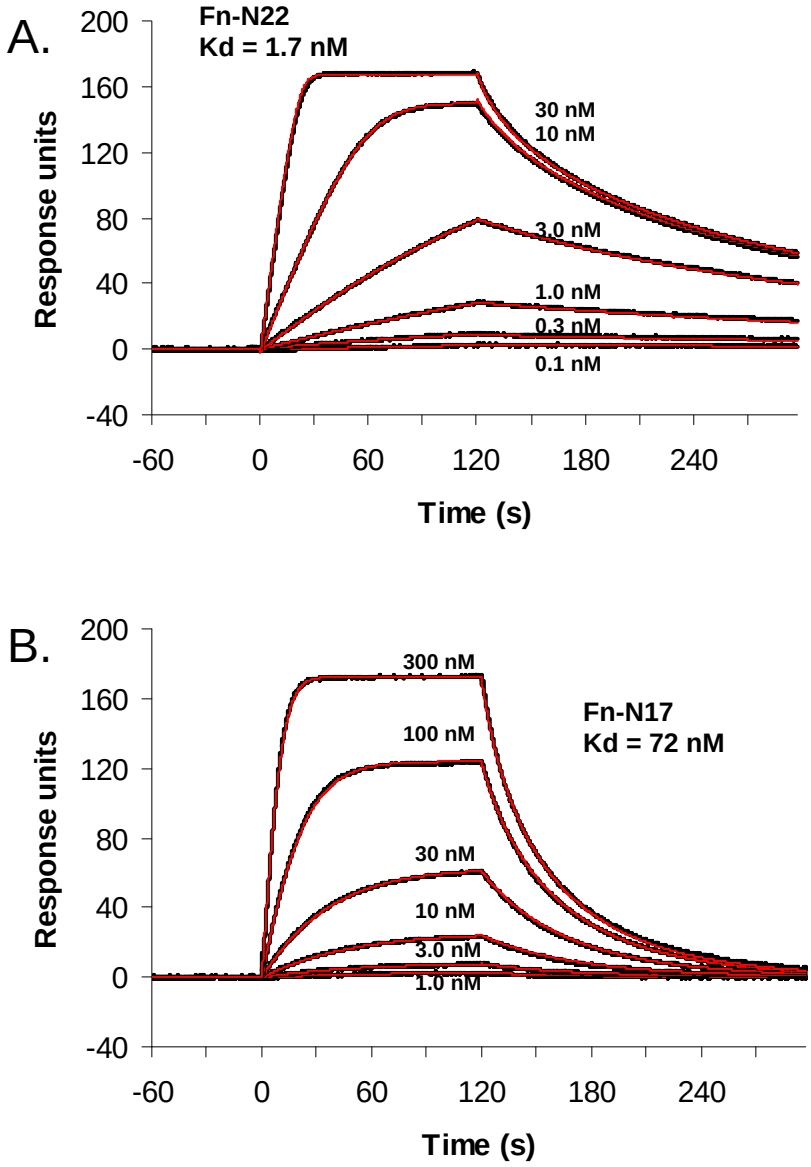

Figure 4.4 Affinity of Fn-N22 (A) **and Fn-N17** (B) **for SARS Nucleocapsid protein.** Determined by surface plasmon resonance with a Biacore T100 instrument. Raw data is in black, fitted curves are red.

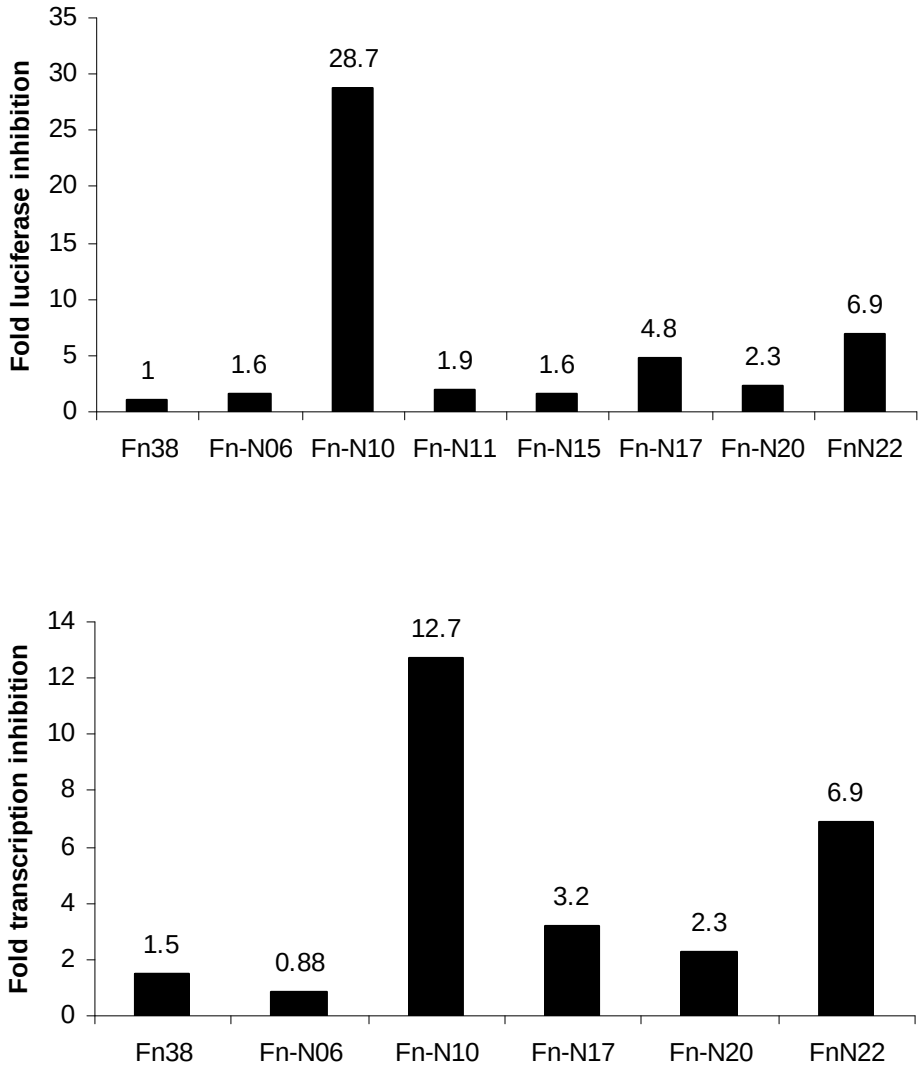

Figure 5. Inhibition of SARS gene expression by intracellular expression of N-binding fibronectins. A) 293T-ACE2 cells were transiently transfected with fibronectins and infected with SARS-CoV RL. Luciferase activity was assayed 20 hours post infection and was normalized to infected cells which were transfected with empty vector. B) 293T-ACE2 cells transiently transfected with fibronectins were infected with wild type SARS-CoV. QPCR was performed to determine relative inhibition of ORF N transcription.

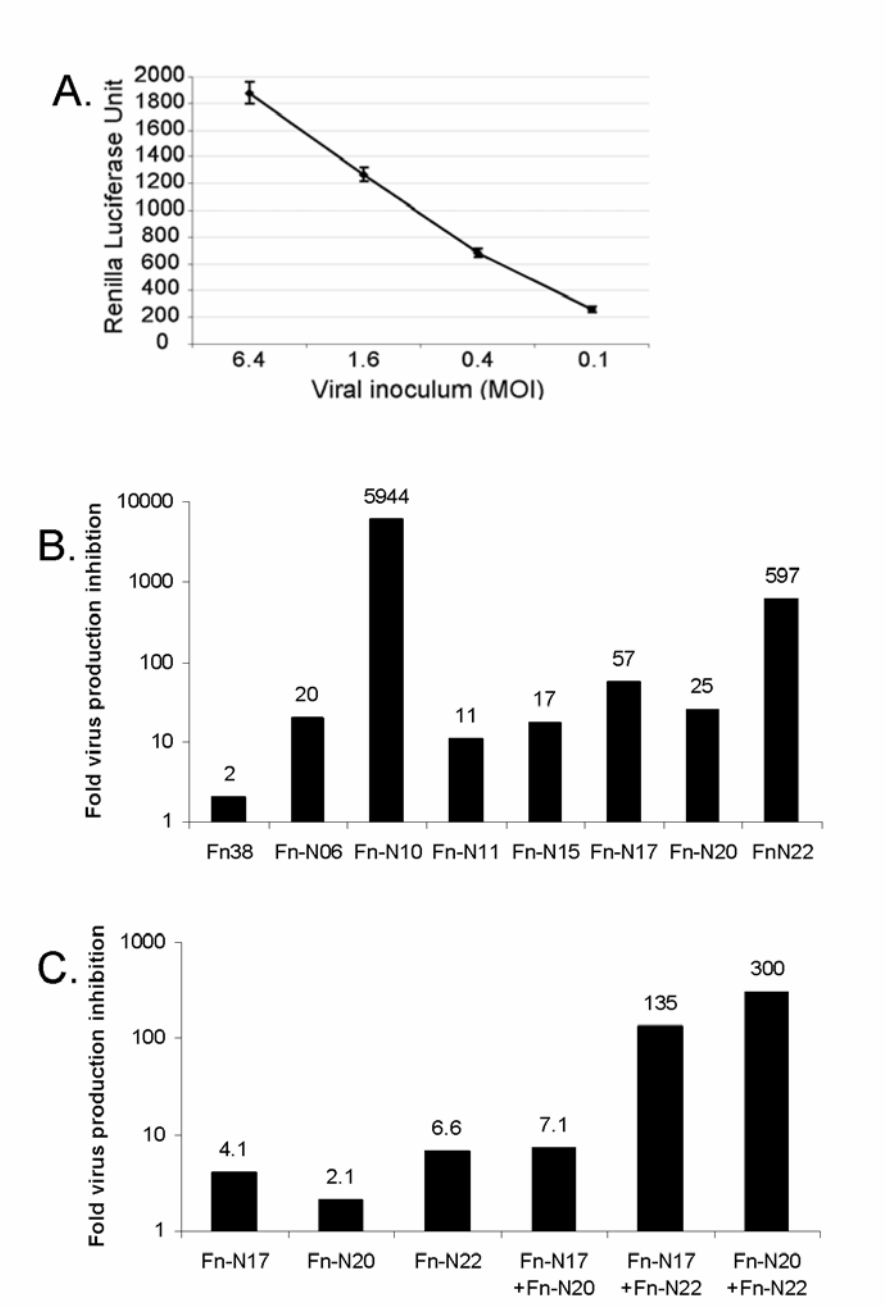

Figure 6. Inhibition of SARS CoV production by intracellular expression of N-binding fibronectins. A) Correlation between viral inoculums and luciferase activity, measured in quadruplicate. B) and C) 293T-ACE2 cells were transfected with pIRES-fibronectins and infected with SARS-CoV RL. The cell culture supernatants were collected 16 hours post infection and used to infect non-transfected cells for amplification of virus. Luciferase activities were determined and normalized to activity of amplified virus from cells initially transfected with empty vector.